

RESEARCH ARTICLE

10.1002/2017JC013728

Surface Drifter Observations From the Arctic Ocean's Beaufort Sea: Evidence for Submesoscale Dynamics

Special Section:

Forum for Arctic Modeling and Observational Synthesis (FAMOS) 2: Beaufort Gyre Phenomenon

J. A. Mensa¹ , M.-L. Timmermans¹ , I. E. Kozlov^{2,3} , W. J. Williams⁴, and T. M. Özgökmen⁵ 

¹Department of Geology and Geophysics, Yale University, New Haven, Connecticut, USA, ²Russian State Hydrometeorological University, St. Petersburg, Russia, ³Marine Hydrophysical Institute of RAS, Sevastopol, Russia, ⁴Institute of Ocean Sciences, Fisheries and Oceans Canada, Sidney, British Columbia, Canada, ⁵Rosenstiel School of Marine and Atmospheric Science, University of Miami, Miami, Florida, USA

Key Points:

- Surface drifters provide observational evidence for submesoscale flows in the Beaufort Sea
- Submesoscale flow features in the mixed-layer drive drifter separation and lateral transport
- Dispersion of drifters is consistent with the presence of a forward-cascade inertial range

Correspondence to:

J. A. Mensa,
jean.mensa@yale.edu

Citation:

Mensa, J. A., Timmermans, M.-L., Kozlov, I. E., Williams, W. J., & Özgökmen, T. M. (2018). Surface drifter observations from the Arctic Ocean's Beaufort Sea: Evidence for submesoscale dynamics. *Journal of Geophysical Research: Oceans*, 123. <https://doi.org/10.1002/2017JC013728>

Received 21 DEC 2017

Accepted 13 MAR 2018

Accepted article online 26 MAR 2018

Abstract Position and velocity data are analyzed from a release of surface ocean drifters in the Arctic Ocean's Beaufort Sea in ice-free conditions. Position information is returned at sufficiently high frequency to allow for the investigation of surface-ocean flows ranging from around 0.5 km in lateral scale (submesoscale, SM, flows) to flows that are tens of kilometers in horizontal extent. Lagrangian statistics from the drifter release are analyzed in conjunction with Eulerian (ship-based) measurements of surface ocean temperature and salinity. Results show dynamics that are largely consistent with flows at similar scales in the midlatitude oceans. Horizontal wavenumber k spectra of density in the surface ocean scale as k^{-2} , consistent with energetic SM flows. Lagrangian drifters indicate *local* dispersion in the surface ocean layer at horizontal scales smaller than 10 km, which confirms the presence of active submesoscale dynamics. Features at these scales give rise to lateral diffusivities (in the range $1-10^3 \text{ m}^2 \text{ s}^{-1}$) of similar range to values inferred in the midlatitudes. Velocity structure functions present an energy-cascade inertial range at submesoscales with indication of a transition to a forward energy cascade at scales smaller than 1 km confirming the transition to 3-D turbulence. The active SM flow-field drives enhanced lateral and vertical fluxes in the Arctic Ocean mixed layer, which has first-order implications to the transport of heat, sea-ice floes, nutrients, and contaminants.

Plain Language Summary Transport and distribution of pollutants and biogeochemical tracers is driven by currents in the upper ocean. Surface-ocean observations in the midlatitudes, as well as numerical modeling, have shown that small-scale flows (i.e., submesoscale flows) play a key role in this transport. Here we present results from a drifter release experiment in the Arctic Ocean's Beaufort Sea. Results provide in-situ observational evidence, for the first time, for the presence of submesoscale flows in the Beaufort Sea. These results extend observations of submesoscale flows in the midlatitude oceans, and improve understanding of the Arctic Ocean system where the transport and distribution by submesoscale flows of ocean heat and sea-ice floes are of climate significance.

1. Introduction

The mixed layer of most ocean basins has been shown to be populated by small-scale ageostrophic features-submesoscale (SM) flows (Callies et al., 2015; Capet et al., 2008a, 2008b; Luo et al., 2016; Mensa et al., 2013; Sasaki et al., 2014; Veneziani et al., 2004). These are features characterized by Rossby and Richardson numbers $\mathcal{O}(1)$ and horizontal length scales ranging from a few hundred meters to a few kilometers. SM features have been shown to play an important role in the ocean energy cascade (D'Asaro et al., 2011; McWilliams, 2008; Molemaker et al., 2005; Poje et al., 2017), nutrient transport (Klein & Lapeyre, 2009; Mahadevan & Archer, 2000; Mahadevan & Tandon, 2006; Martin & Richards, 2001; Omand et al., 2015), heat transport (Lapeyre & Klein, 2006; Rudnick, 1996) and the lateral dispersion of pollutants (Poje et al., 2014, 2017). This study is an analysis of ocean surface drifter observations to examine SM flows in the Arctic Ocean's Beaufort Sea. SM flows in the Arctic Ocean can be of first-order relevance to sea-ice dynamics and thermodynamics, dispersion of pollutants such as oil, and vertical transports of heat, salt, and nutrients.

Observations in the mixed layer under sea ice indicate the presence of an active upper ocean populated by SM fronts (Timmermans et al., 2012); although these features significantly affect mixed-layer restratification,

they are relatively weak and characterized by steeper horizontal wavenumber spectra of density than typically observed in the midlatitude ice-free oceans. Observations in summer ice-free regions (in the Arctic's Chukchi Sea) have shown similarly steep wavenumber spectra (Timmermans & Winsor, 2013). High-resolution numerical simulation of the small-scale flow field under sea ice over a full annual cycle corroborates the under-ice observations, and indicates that SM instabilities are largely suppressed by shear resulting from ice-ocean stresses; events with stronger SM activity were present in the simulations, but not typical (Mensa & Timmermans, 2017). Natural extensions of these studies include further investigation of SM flows in marginal ice zones where they have the potential to be more active (Manucharyan & Thompson, 2017).

SM flows are rapidly evolving, small-scale processes which are characterized by high values of relative vorticity. This makes them difficult to sample with classic Eulerian approaches. Examples of direct observations of SM features have appeared only recently (Callies et al., 2015; D'Asaro et al., 2011; Shcherbina et al., 2013). One approach that has proven successful in the study of SM flows in the ocean is the use of Lagrangian drifters (Poje et al., 2014). Drifters released in the surface ocean allow for the study of upper ocean flows over a broad range of temporal and spatial scales in a way that is virtually impossible with Eulerian approaches.

Here we explore SM flow dynamics in the Arctic Ocean via Lagrangian drifters which return position information sufficiently frequently for the purpose. We present an analysis of drifter trajectories together with other ship-based measurements from a 2016 experiment in the Beaufort Sea. In the next section, we outline the drifter release and measurements. In section 3, we describe the general oceanographic setting and evolution as the drifters returned position information. In section 4, we compute Lagrangian statistics indicating evidence for SM flows and their role in upper-ocean lateral transport and the energy cascade. Finally, in section 5, we summarize and discuss our results in context with dynamics and lateral transport in the midlatitudes and show SM flows contribute significantly to lateral dispersion and diffusivity in the Beaufort Sea.

2. Drifter Deployment and Supplementary Data

Ocean drifters were deployed from the Canadian Coast Guard Ice Breaker *Louis S. St-Laurent* (LSSL) during the 2016 Joint Ocean Ice Studies (JOIS) expedition in the Beaufort Sea, a collaboration with the Beaufort Gyre Exploration Program (<http://www.whoi.edu/beaufortgyre>). The drifters were developed under the Consortium for Advanced Research on Transport of Hydrocarbon in the Environment (CARTHE), and have been used successfully in a number of experiments in the Gulf of Mexico (e.g., Lumpkin et al., 2017). The drifters are made of biodegradable plastic and consist of a floating torus (35 cm diameter and 8 cm in thickness)

and a submerged component (two square panels of side length 42 cm interlocked together at 90°). The torus and submerged panels are connected by a 15 cm long flexible chain (Novelli et al., 2017). A GPS unit resides in the torus which sits about 3 cm above the water surface (and 5 cm below). The drifter extends to a depth of ~60 cm and is designed to follow the surface-ocean flow field such that the influence of waves and winds is minimized (Novelli et al., 2017). The GPS returns a position every 5 min, accurate to within ~6 m. Data are interpolated to 15 min intervals to reduce noise. This sampling is sufficient to study flow features that evolve over about a day and have spatial scales ranging between $\mathcal{O}(100)$ m and $\mathcal{O}(1)$ km (e.g., see Haza et al., 2014).

In total, 18 drifters were released from the LSSL in ice-free waters on 25 September 2016 in the vicinity of 115°W and 68°N. The drifters returned position information from the ice-free waters for a total of 53 days (the last drifter transmitted its position on 18 November; Figure 1). Drifters were released in six groups of three with the goal of sampling a relatively large area while achieving initially small separation between drifters. The distance between each group was about 100 m (each group was released 1 min apart); in each group, the three drifters were initially separated by less than about 20 m. The drifter

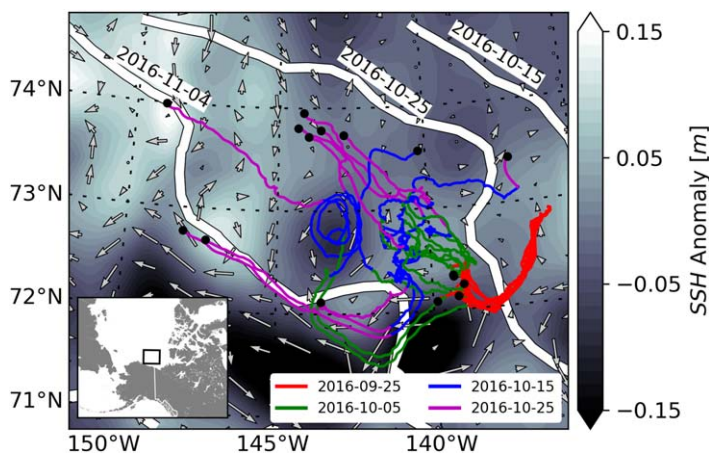


Figure 1. Drifter trajectories from the release location to final positions (shown by black dots). White lines represent the ice edge at 10, 20, and 30 days from drifter release; drifter trajectories are color-coded for the same periods. Sea-surface height (SSH) anomaly (m) for 15 October is color contoured and white vectors indicate derived geostrophic velocities; the SSH product has a temporal resolution of 1 day and a spatial resolution of 0.25°.

deployment was done along a straight line of total length $\sim 1,200$ m and took ~ 5 min to complete, making it effectively simultaneous.

Drifters returned position information for an average of 22.3 days, with 6 drifters transmitting for less than 5 days, one drifter transmitting for 53 days, and 11 drifters transmitting for 20 days or longer. For the analysis, drift trajectories were clipped to 30 days after which point most drifters had stopped transmitting, presumably compromised by growing sea ice. One of the drifters lost its drogue during the deployment, and its movement is expected to be primarily driven by wind and waves (based on laboratory tests (Novelli et al., 2017)). This drifter was removed from the analysis, although we later compare its behavior to that of the other drifters.

In addition to the drifter trajectories, several other data sources are used in this study. Over the period of the drifter deployment, LSSL shipboard measurements were made of salinity and temperature (both from an underway ship-based system for measurements in the surface ocean, and from hydrographic CTD profiles). Atmospheric data from the region were taken from NCEP Reanalysis provided by NOAA/OAR/ESRL PSD, Boulder, Colorado (available at <http://www.esrl.noaa.gov/psd/>). Geostrophic currents are derived from altimetry measurements of sea-surface height (SSH) anomaly produced and distributed by the Copernicus Marine and Environment Monitoring Service (CMEMS, <http://www.marine.copernicus.eu>). This product is the assimilation of a suite of altimetry measurements as outlined here: http://marine.copernicus.eu/wp-content/uploads/2016/06/r2637_9_cmems3468_l4_products.pdf. For a few days during the drifter deployment, Synthetic Aperture Radar (SAR) imagery was available with data acquired by the Sentinel-1B satellite and distributed by Copernicus Open Access Hub (<https://scihub.copernicus.eu>).

3. Drifter Behavior and Oceanographic Setting

For the first week following the release, drifters remained in close proximity to one another with little divergence (Figure 1). Even after the group begins to diverge, the drifters in general transit to the west (average drifter speeds were in the range 0.2 m s^{-1}), advecting in the main anticyclonic Beaufort Gyre circulation (e.g., Proshutinsky et al., 2009). Trajectories show the clear signal of (clockwise) inertial oscillations with the inertial period being about 1/2 day at these latitudes (Figure 2, bottom panel); in general, all drifters showed a rather continuous inertial signal over the duration, and clockwise loops in the drift trajectories are a consistent feature. Over the entire duration of the experiment, winds remained around 5 m s^{-1} with the exception of a few events with winds up to 10 m s^{-1} (Figure 2, top panel). We can corroborate the extensive laboratory testing of these drifters, which indicates that they present only little windage (Novelli et al., 2017); we find a correlation between wind and drifter velocity components to be about 0.2 for all drifters. This low correlation is in contrast with a correlation of about 0.6 between the velocity components of the drogue-less drifter and wind velocity components.

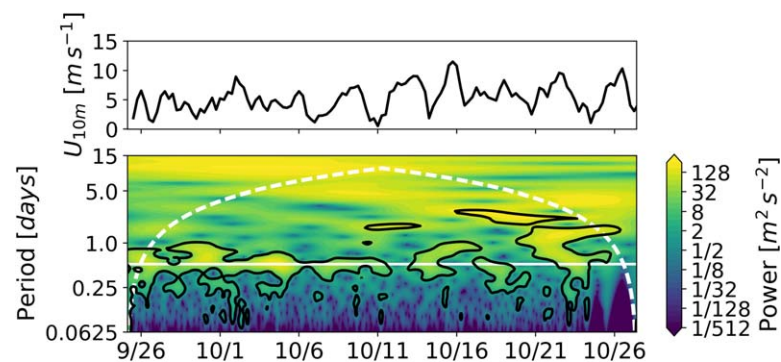


Figure 2. Drifter velocity wavelet (lower panel) computed for a single drifter (all other drifters indicate a similar signal), where the color represents the power amplitude of the drifter speed on a log-scale. The wavelet is computed using a 30 day time series; the cone of influence (white dashed line) indicates the region outside of which edge effects become important. The white solid line corresponds to the inertial frequency, ~ 0.5 day at these latitudes. The black contour marks regions with confidence level of 95%. The top panel shows wind velocity time series computed by interpolating NCEP data to the drifter location.

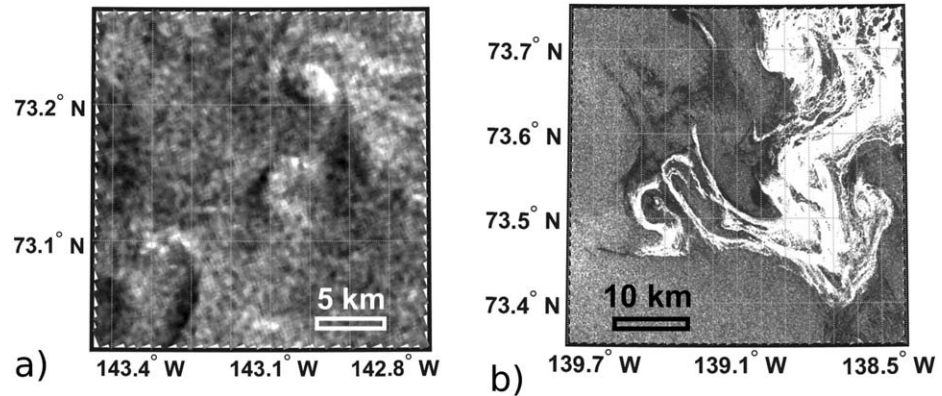


Figure 3. SAR snapshots from 15 October (Copernicus Sentinel data (2017)) showing (a) submesoscale eddies to the north east of a mesoscale eddy at 72.5°N and (b) detail of the ice edge identified as white regions due to high radar reflectivity.

Around 9–10 days after the 25 September release, the drifters began to separate more rapidly. At this time, two drifters separated from the group and began to loop around a mesoscale eddy ~ 40 km in diameter, while the other drifters remained free from the influence of such larger-scale features (Figure 1). A SAR image from 15 October (Figure 3), 20 days after release, shows a variety of ocean features suggesting the possibility of SM instabilities in the study region. The boundaries of the mesoscale eddy and other regions present numerous smaller-scale eddies (~ 5 km in diameter) and filaments (Figure 3a). The SAR image also illustrates ice floes (Figure 3b) that are organized in elongated structures and filaments suggesting the presence of submesoscale features developing at the marginal ice zone.

For the duration of the experiment, surface fluxes were predominantly negative (i.e., cooling) with cooling of around -80 W m^{-2} , observed at the start of the experiment (25 September), and maximum cooling of about -260 W m^{-2} observed during the night of 13 October. Through the month of October, the mixed layer progressively cools toward freezing temperature and this is accompanied by the onset of sea-ice growth. At the time and location of the drifter release, ship-based temperature and salinity profiles indicate mixed-layer temperatures above freezing and mixed-layer depths ~ 30 m (Figure 4a). Another CTD profile was taken at the same location 18 days later (on 13 October), at which time the mixed layer was cooler and saltier (as a result of brine fluxes and possibly also shear-driven mixing, although there was no appreciable change in mixed-layer depth between the earlier and later profiles, Figure 4a). During the experiment, the marginal ice zone migrated from northeast to southwest as fall freeze-up progressed (Figure 1). By the end of October, drifters appear to be surrounded by a newly growing and deforming sea-ice pack, and are perhaps frozen-in or otherwise compromised; whatever the case, in the field of growing sea ice, the drifters ultimately fail to transmit position information.

Temperature and salinity measurements from an underway system on the LSSL, sampling extensively in the drift area, provide useful constraints on the surface-ocean flow field (Figures 4b and 4c). Water from around 10 m depth was sampled every 30 s, to yield a horizontal resolution of around 200 m for typical ship speeds. At these cold temperatures, temperature T variations have negligible effect on the density and density variations (not shown) resemble salinity S variations along the ship track (Figure 4c). Lateral $T - S$ variations are generally small along the ship track, with a few notable exceptions. A significant deviation to warmer, fresher water (near the start of the red segment, Figures 4b and 4c, top panel) is associated with the presence of coastal influxes near the mouth of the Mackenzie River. We also observe the transition from fresher waters associated with the Beaufort Gyre to warmer, saltier waters toward the shelf boundaries (the green segment, Figures 4b and 4c, middle panel). A similar increase in salinity moving from the Beaufort Gyre interior toward the margins is also apparent in the blue segment (Figures 4b and 4c, bottom panel). Although underway measurements of surface salinity and temperature are expected to be somewhat affected by the influence of the ship on the mixed layer, we find time series measurements from the underway system are in generally good agreement with concurrent mixed-layer measurements from CTD profiles.

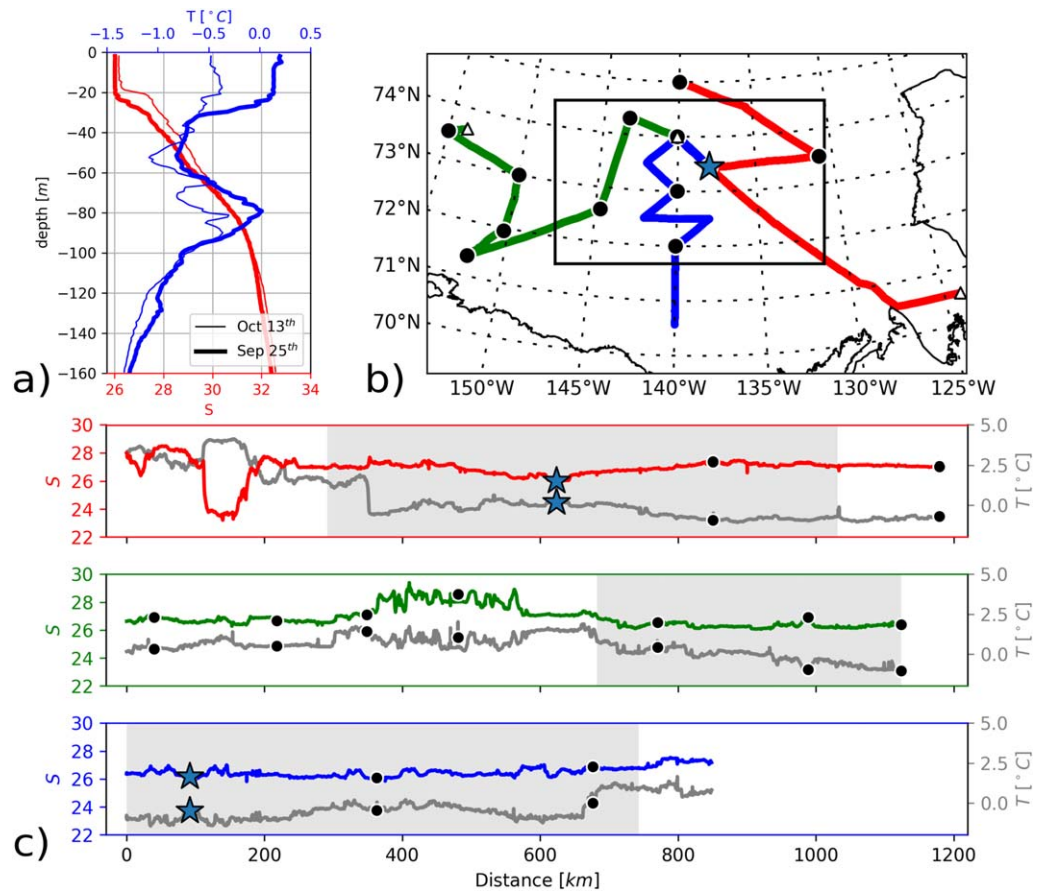


Figure 4. (a) Ship-based CTD profiles: temperature, T ($^{\circ}\text{C}$, blue) and salinity, S (red) versus depth profiles taken at the star in panels (b) and (c). The same station was sampled twice at two different times (thinner and thicker lines). (b) Map showing portions of the LSSL ship track, where the color-coded segments correspond to the colors in panel (c). Black dots represent locations of hydrographic CTD profiles, the white triangles represent the first point of each segment and the star on the red segment corresponds to the CTD profile taken the same day and a few kilometers away from the drifter release. The black box denotes the region over which the wavenumber spectra are computed (Figure 5). (c) Temperature $^{\circ}\text{C}$ and salinity at 10 m depth from the underway system for the three segments in panel (b): red segment, top panel; green segment, middle panel; and blue segment, bottom panel. The grey shaded portions mark those within the black box shown in panel (b). Black dots mark surface temperature and salinity from the CTD profiles at locations shown in panel (b). The underway $T - S$ values are in good agreement with the CTD values.

The underway $T - S$ measurements allow us to compute horizontal wavenumber k spectra of density variance along the track (Figure 5). The spectra are computed on three separate portions of the ship track (and then averaged) after interpolation of the nominally 200 m spaced measurements to a regular 250 m spacing. The smallest resolved scale is then 500 m. The largest scales accessible are several hundred kilometers. The spectrum has a slope of $k^{-2.02}$ in good agreement with the k^{-2} scaling typical of surface-intensified frontal activity and SM dynamics (Callies et al., 2015). Unlike passive tracers, where for 2-D turbulence k^{-1} scaling is expected, properties such as buoyancy have the same spectral slopes as kinetic energy. This has been shown in numerical simulations (Capet et al., 2008a), observations (Callies et al., 2015), and via theoretical considerations (Blumen, 1978). Wavenumber spectra under sea ice (Timmermans et al., 2012) in the region of our study indicated steeper spectra than the $k^{-2.02}$ found here, suggestive of weaker SM dynamics under sea ice. The reason for only weak SM activity under sea ice has been attributed largely to the presence of ice-ocean shear (Mensa & Timmermans, 2017).

Wavenumber spectra of density variance and kinetic energy are valuable for understanding the energetics (and energy cascade) of the flow field; however, producing useful spectra is often limited by the spatial and temporal scales accessible in the sampling approach. Alternatively, it is possible to gain additional insights into the turbulent field from a Lagrangian approach.

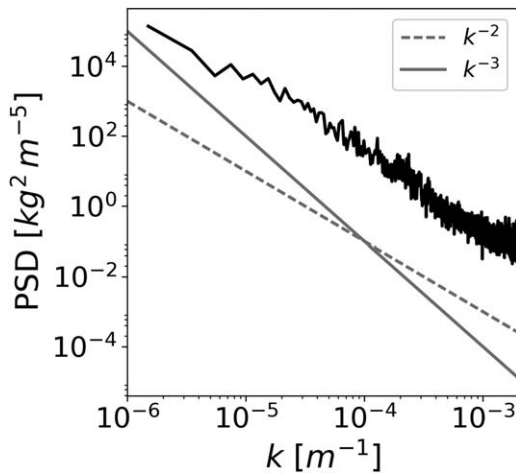


Figure 5. Horizontal wavenumber k spectra of density variance computed from the $T-S$ measurements from the LSSL underway system. Spectra are computed using the portion of the record enclosed in the black box (i.e., the main drift region) shown in Figure 4b, and delineated by the grey shading in Figure 4c. Spectra are computed independently for each colored segment in Figure 4b (of length 740, 441, and 742 km, respectively) and then averaged together. The best fit slope for the resulting spectrum is $k^{-2.02}$ while the individual spectra had slopes $k^{-1.96}$, $k^{-2.02}$, and $k^{-1.94}$, respectively.

2017); SM flows characterized by frontogenesis are expected to scale more like k^{-2} (Boyd, 1992; Callies et al., 2015).

The properties of the energy/enstrophy cascade can be diagnosed via both Lagrangian statistics and Eulerian diagnostics. The horizontal wavenumber spectrum of density presented (Figure 5) shows a k^{-2} slope consistent with surface-intensified SM flows (Callies et al., 2015). However, the spatial resolution of the underway $T-S$ measurements is insufficient to investigate the properties of flows smaller than 500 m lateral scale, close to where the transition to a forward energy cascade would be expected. Analysis of the Lagrangian drifter motions, however, does allow for the investigation of this transition from nearly 2-D to 3-D flows.

The presence of an inertial range in the observed flow field can be identified and further explored via the study of relative dispersion and velocity structure functions. We begin in the following section by quantifying relative dispersion; relative diffusivity is also estimated as this allows for convenient comparison with previous studies.

4.1. Relative Dispersion and Diffusivity

Relative dispersion, $\sigma_r^2(t)$, may be defined as the separation between drifter pairs averaged over all drifters at any given time, $\sigma_r^2(t) = \langle (\mathbf{x}(t)_i - \mathbf{x}(t)_j)^2 \rangle$, where $\langle \cdot \rangle$ represents averaging over all drifter pairs, i and j subscripts denote each of the two drifters in a pair, and $\mathbf{x}(t)$ is drifter position at time t . $\sigma_r^2(t)$ is computed as a function of time over the duration of the experiment (Figure 6a). During the first day after drifter release separation takes place as $\sigma_r^2 \propto e^t$. At this time, dispersion is driven by features with length scales larger than the drifter separation length scale (i.e., it is *nonlocal*). After about a day, dispersion transitions to the Richardson regime, with $\sigma_r^2 \propto t^3$ (Richardson, 1926). Dispersion in this regime is driven by features having scales similar to drifter separation scales (i.e., it is *local*). This regime characterizes an inertial range with a self-similar energy cascade (consistent with Figure 5) although no information can be extracted as to whether this is due to a 2-D or 3-D flow field; to answer this, we compute Lagrangian structure functions (section 4.2).

To assess the sensitivity of the relative dispersion estimates to the number of drifters deployed, we compute relative dispersion after removing two drifters (equivalent to $\sim 10\%$ of the drifters) at a time from the original pool of drifters. The grey lines in Figure 6a show the maximum and minimum values of σ_r^2 with two removed drifters for 100 random extractions. While increasing the number of drifters would reduce

4. Lagrangian Statistics

Lagrangian diagnostics can be used to investigate turbulent properties of the flow field underlying the movement of the drifters (LaCasce, 2008). In particular, it is possible to distinguish between two-dimensional and three-dimensional flows and their corresponding energy/enstrophy cascades. Mesoscale ocean flows having lateral scales larger than around 10 km (corresponding to the scale of the first baroclinic deformation radius in the Canada Basin halocline, Zhao et al., 2014) are approximately 2-D, while submesoscale ($\mathcal{O}(1)$ km lateral scales) flows tend toward 3-D. In classic 3-D turbulence, a self-similar inertial range characterizes the transition between an injection scale (at the large scale) and a dissipation scale, the smallest scale (Kolmogorov, 1991). Kinetic energy E flows toward smaller scales (a forward cascade) along a constant slope with $E \sim k^{-5/3}$. In 2-D turbulence, two cascades emerge around the injection: a backward energy cascade with slope $k^{-5/3}$ and a forward enstrophy cascade with slope k^{-3} . While large scale ocean flows are expected to be mostly 2-D, a transition toward 3-D turbulence is expected at sufficiently small scales. This transition has been suggested to be at the scale of SM flows where instabilities emerging from the breakdown of frontal structures lead to the transition to 3-D turbulence (D'Asaro et al., 2011; McWilliams, 2008; Molemaker et al., 2005; Poje et al.,

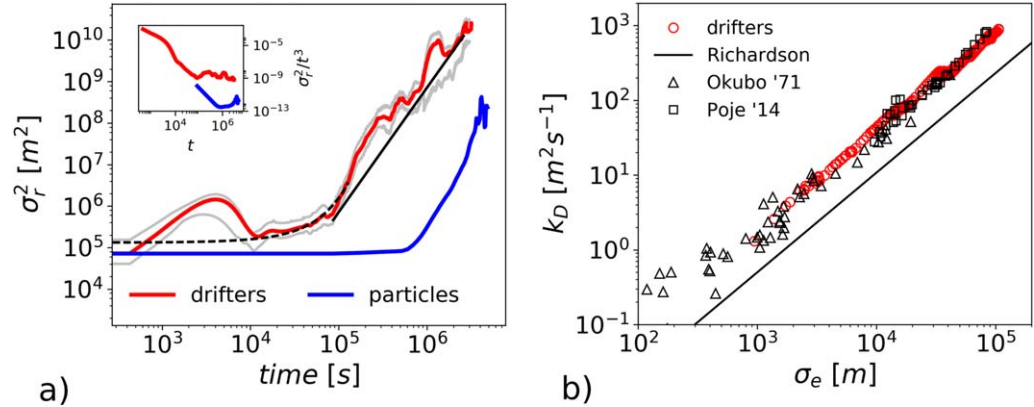


Figure 6. (a) Relative dispersion (σ_r^2 (m^2)) time series for drifters (red) and synthetic particles (blue) advected by geostrophic velocities derived from SSH fields. Grey lines represent limiting relative dispersion curves computed after removing two drifters ($\sim 10\%$ of the total). Best fit lines are shown for exponential separation ($\sigma_r^2 \propto e^t$, black dashed line) and Richardson scaling ($\sigma_r^2 \propto t^3$, solid black line). The inset is relative dispersion scaled over time (σ_r^2/t^3) shown in order to highlight the Richardson scaling regime. (b) Scale-dependent relative diffusivity, $k_D = \sigma_e/4t$ ($\text{m}^2 \text{s}^{-1}$), versus σ_e computed by fitting ellipses to the drifter distribution. k_D is compared to lateral diffusivity inferred from previous drifter and dye release studies.

uncertainty, it appears that the qualitative properties of relative dispersion slopes and regime transitions are approximately preserved over the range of drifter numbers tested here.

It is instructive to compute relative dispersion using synthetic particles advected by geostrophic velocities derived from the SSH fields; this allows us to contrast the drifter dispersion with dispersion of particles advected by a nearly 2-D flow field where SM features are not resolved; this allows us to contrast the drifter dispersion with dispersion of particles advected by a nearly 2-D flow field where SM features are not resolved. We release particles in the same region as the drifters and with the same initial relative dispersion (i.e., specifying the initial separations of particles to be consistent with those of the drifters) but in much larger numbers (a total of 1,000 synthetic particles are released). The SSH 24 hourly field with a spatial resolution of 0.25° (about 10 km) is used here. Particles are released on 25 September and are advected for 30 days (i.e., the same duration as the real drifters). Velocities at the particle locations are determined through linear interpolation of the SSH grid.

It takes at least several days longer for σ_r^2 estimated from the synthetic particles to take on scaling equivalent to that obtained from the drifters (Figure 6a). Dispersion is nonlocal ($\sigma_r^2 \propto e^t$) for a significant fraction of the time series obtained from the synthetic particles, and Richardson scaling is realized only toward the end of the time series (Figure 6a). This can be explained by the fact that particles are under the influence of a nearly 2-D geostrophic flow field which is characterized by transition from an enstrophy cascade at small scales, identifiable by particles satisfying $\sigma_r^2 \propto e^t$, to backward energy cascade characterized by Richardson scaling, $\sigma_r^2 \propto t^3$. Notice nevertheless that dispersion statistics are significantly affected by the initial scale of separation of the particles (Babiano et al., 1990) as well as by the temporal and spatial resolution limitations of the SSH field; initial separation of the particles is *subgrid* and thus inevitably nonlocal.

It is of interest to note that dispersion can present locally steeper scaling than the theoretical t^3 Richardson scaling (Figure 6a); this is evidenced also in numerical results (Mensa et al., 2015). This may be explained by the presence of intermittent forcing on the flow field, which can generate deviations from Richardson scaling (Babiano et al., 1990; Curcic et al., 2016). These deviations to larger slope are less apparent in another study (Poje et al., 2014), where a larger number of drifters were analyzed and local intermittency attenuated.

Measurements of dispersion can be conveniently used to compute scale-dependent relative diffusivity k_D which allows both for a comparison with results of previous ocean observations, as well as insight into the values of lateral diffusivity expected in the surface layer of the Beaufort Sea. Scale-dependent diffusivity is computed as $k_D = \sigma_e^2/4t$ (Okubo, 1970), where σ_e^2 is cloud dispersion computed by fitting ellipses to the drifter field, $\sigma_e^2 = 2 \sigma_M \sigma_m$, where σ_M and σ_m are the major and minor axes of the ellipses, respectively. The

ellipses represent the two principal components of the drifter distribution and are effectively a measure of the standard deviation of the locations around the center of mass of the entire drifter cloud. Ellipses and the corresponding values of k_D are computed at each time step (i.e., 15 min interval). Via analyses of smoke plume observations, k_D in the inertial range was shown to scale as $k_D \sim l^{4/3}$ where l is the length scale of particle separation $l = \sigma_e$ (Richardson, 1926). This is the Lagrangian equivalent to the Eulerian inertial range (Kolmogorov, 1941). Values of k_D obtained here are compared against a collection of diffusivity measurements from dye release experiments collected in a variety of settings (from lakes to the open ocean) (Okubo, 1970), drifters deployed in the Gulf of Mexico (Poje et al., 2014) and theoretical Richardson scaling (Figure 6b). Diffusivity from drifters is computed every 6 h (subsampling the time series for clarity in the panel), beginning 2 days after release (in order to select local dispersion). Scale-dependent diffusivities from the surface Beaufort Sea are in good agreement with those estimated in midlatitude studies, which implies that we can expect significant lateral dispersion of tracers and pollutants in the Beaufort Sea. Moreover, the presence of Richardson scaling extending into the SM regime implies that lateral diffusivity is scale dependent and that all scales up to $\mathcal{O}(1)$ km present distinct values of lateral diffusivities. This also suggests that it is not reasonable to specify a single eddy diffusivity coefficient in models, but rather a scale-dependent diffusivity should be considered.

4.2. Second-Order and Third-Order Structure Functions

While the Richardson scaling result for relative dispersion and diffusivity (Figures 6a and 6b) is consistent with an inertial range, it does not imply the presence of a dynamic cascade; similar slopes can be found for purely kinematic flow fields without a real turbulent cascade (Nicolleau & Nowakowski, 2011; Thomson & Devenish, 2005). Further insights into the properties of the turbulent field experienced by the drifters can be obtained from the study of longitudinal velocity increments defined as

$$\Delta u_l(r, t) = (\mathbf{u}(\mathbf{x} + \mathbf{r}, t) - \mathbf{u}(\mathbf{x}, t)) \cdot \frac{\mathbf{r}}{\|\mathbf{r}\|},$$

where \mathbf{r} is the distance between pairs of drifters. The n th-order structure functions are defined as $S_u^n(r) = \langle \Delta u_l^n \rangle$, where the angle brackets represent averaging over uniform separation intervals and in time. The structure functions are effectively a measure of the velocity correlation between drifter pairs as a function of distance and time. We compute $\Delta u_l(r, t)$ on the assumption that drifter pairs measure instantaneous Eulerian velocity; as such, sampling biases and limited drifter numbers introduce uncertainty. Nevertheless, we will show how the main characteristics of the turbulent flow field are captured here. While diagnostics present significant scatter (especially at the small scale), the agreement with the theoretical prediction is good.

The second-order structure function $S_u^2(r)$ can be used to infer the presence of either an energy or enstrophy cascade (see Poje et al., 2017). For an enstrophy cascade, as in 2-D turbulence, $S_u^2(r)$ takes the form $S_u^2(r) = C_n \nu^{2/3} r^2$, where ν is the enstrophy cascade rate (with units s^{-3}) and C_n is a dimensionless constant. Conversely, for an inertial range (in both 2-D and 3-D turbulence), $S_u^2(r) = \tilde{C}_n (\epsilon r)^{2/3}$, where ϵ is the energy cascade rate (with units $m^3 s^{-2}$) being positive in the case of a forward energy cascade, or negative in the case of a backward cascade, and \tilde{C}_n is a dimensionless constant.

The scaled second-order structure function, $S_u^2(r)/r^2$, exhibits a $r^{-4/3}$ scaling for the drifters and zero-slope for the synthetic particles (Figure 7a). This suggests the presence of an energy cascade inferred from the drifters and an enstrophy cascade inferred from the particles. Analysis of the synthetic particle distribution indicates a change in slope at scales around 20 km (i.e., scales comparable to the first baroclinic deformation radius; Figure 7a). There exists the possibility that this is associated with the transition (at the meso-scale) in the 2-D energy spectrum from a forward enstrophy cascade to a backward energy cascade. It is possible to gain insight into the Eulerian properties of the flow field underlying the drifter-inferred energy cascade by computing the fluctuating Rossby number $Ro^2 = \frac{S_u^2(r)}{f^2 r^2}$ (Poje et al., 2017). Using a value for the Coriolis parameter f around the latitude of the drifter release, $f = 1.4 \times 10^{-4} s^{-1}$ and considering scales $r = 1$ km and $r = 250$ m, yields $Ro_{1km} = 0.5$ and $Ro_{250m} = 1.4$, respectively. These values are consistent with high values of the Rossby number expected for submesoscale features.

The second-order structure function does not provide the direction of the energy cascade. In 2-D and geostrophic turbulence, this cascade is backward, while for 3-D turbulence, it is forward. In order to investigate

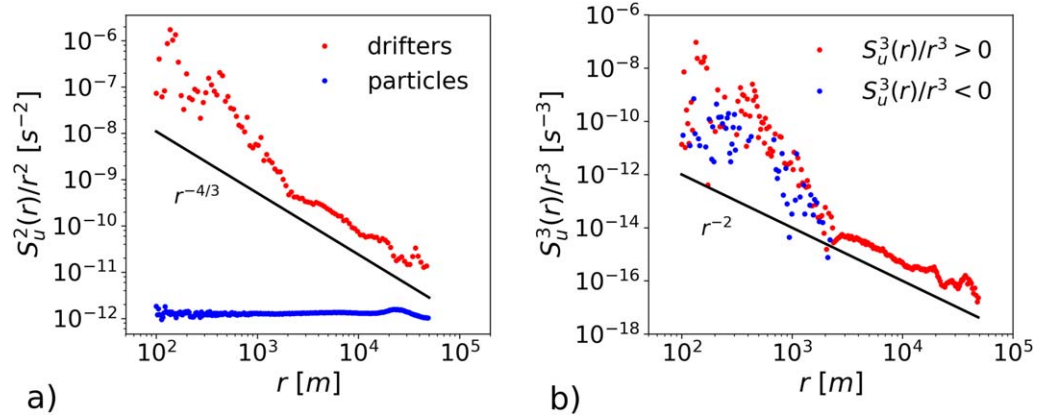


Figure 7. (a) Scaled second-order structure function, $S_u^2(r)/r^2$ (s^{-2}), versus length scale r (m) computed for both the drifters and synthetic particles. (b) Scaled third-order structure function $S_u^3(r)/r^3$ (s^{-3}) versus length scale r (m) computed for drifters only. The lines $r^{-4/3}$ and r^{-2} (panels (a) and (b), respectively) represent the nominal slopes for the inertial range. Negative values are shown in panel (b) by inverting the sign of the structure function (see legend).

whether dynamics are diverging from quasigeostrophic balance into 3-D turbulence and a forward energy cascade (as is expected for SM flows), we compute the scaled third-order structure function, $S_u^3(r)/r^3$ (Figure 7b). According to Kolmogorov's 4/5th law, $S_u^3(r)$ for 3-D flows takes the form, $S_u^3(r) = -\frac{4}{5}\epsilon r$, with $\epsilon > 0$ for a forward energy cascade. Results for the drifters show significant scatter at length scales smaller than about 1 km, and confirm a positive energy cascade ($S_u^3(r) < 0$) at these scales. For length scales larger than about 1 km, $S_u^3(r) > 0$, indicative of a backward energy cascade. This is consistent with SM flows, and departure from the thermal wind balance via secondary instabilities and 3-D turbulence (McWilliams, 2008). Scale dependence of the r^3 normalized third-order structure function again confirms the presence of an inertial range with a slope of r^{-2} .

To summarize, in the surface Beaufort Sea, relative dispersion time series suggest the presence of an inertial range and energy cascade ($\sigma_r^2 \propto t^3$), possibly preceded by an enstrophy cascade ($\sigma_r^2 \propto e^t$) (Figure 6a). This is confirmed by the scaled second-order structure function which shows scaling consistent with an energy cascade (Figure 7a). The direction of the energy cascade is then examined using the third-order structure function, which indicates a forward energy cascade ($S_u^3(r) < 0$) for scales smaller than around 1 km. These results confirm the presence of SM flow dynamics, and a transition to 3-D turbulence characterized by a forward energy cascade.

5. Summary and Discussion

This study presents the first analysis of a high-resolution Lagrangian drifter release, analyzed in conjunction with Eulerian measurements of the surface ocean, in mostly ice-free conditions in the Beaufort Sea. Drifters tracked ocean surface currents for 30 days, sampling features spanning the mesoscales to scales as small as $\mathcal{O}(10)$ m. Ship-based T and S collected in the surface ocean layer in the drifter-release region are characterized by a wavenumber spectrum of density with a k^{-2} slope, indicative of frontogenesis typically observed in the midlatitudes (Callies et al., 2015). This structure contrasts with numerical and direct observations of surface flows under sea ice which do not present significant energy at the SM range of the spectrum (Mensa & Timmermans, 2017; Timmermans et al., 2012).

At scales larger than about 1 km, drifter separation, quantified by $\sigma_r^2(t)$ ($\sigma_r^2 \sim 10^6 m^2$ for lateral scales of ~ 1 km), transitions from an exponential behavior ($\sigma_r^2 \propto e^t$) to the Richardson (local) regime ($\sigma_r^2 \propto t^3$). The Richardson regime, where relative dispersion is driven by features at the scale of the drifter separation, extends well into the characteristic scales of mesoscale features. This is an indication of a flow field populated by SM features which drive drifter separation and lateral transport. To better underline the role of SM flows, we analyzed the statistics of synthetic particles advected by SSH-derived geostrophic currents. These particles show significantly slower separation than the drifters, with particles presenting $\sigma_r^2 \propto e^t$ for scales extending well into the mesoscales, as expected for a flow with no SM dynamics. Lateral diffusivities

(computed from cloud dispersion of the drifter set) show similar magnitude and scaling as in several midlatitude studies.

Through examination of velocity structure functions we infer an energy cascade for scales between 100 m and ~ 10 km, and a transition at scales around 1 km from a backward (toward large scales) to a forward (toward small scales) energy cascade. Further, the fluctuating Rossby number takes values of $Ro \sim \mathcal{O}(1)$ at scales of 0.5 km. These results suggest that SM dynamics are active in the surface Beaufort Sea in open water. SM features are known to develop strong vertical velocities responsible for significant vertical property fluxes. That is, SM flows may significantly enhance ocean-to-ice heat fluxes, and also nutrient fluxes into the mixed layer. The presence of an active submesoscale flow field further has implications to the energy budget of the Beaufort Gyre, suggesting a surface pathway for dissipation of wind-energy input. This study highlights the need for a field experiment that could provide information through the full seasonal evolution of sea-ice growth and decay (a transition from open water to sea-ice covered). A tracer release experiment would be valuable, allowing for the identification of vertical transport associated with SM flows. High-resolution numerical simulations will also be necessary to further identify and describe the physics, evolution and implications of SM flows over a range of sea-ice conditions in the Arctic Ocean. We are grateful for valuable discussions during the Forum for Arctic Modeling and Observational Synthesis (FAMOS), and thank Andrey Proshutinsky for helpful comments.

Acknowledgments

This research was made possible by a grant from The Gulf of Mexico Research Initiative. Data are publicly available through the Gulf of Mexico Research Initiative Information & Data Cooperative (GRINDC) at <https://data.gulfresearchinitiative.org> (<https://doi.org/10.7266/N7J9645Q>). The drifter deployment was made possible, and hydrographic data were made available, by the US/Canada collaboration under the Joint Ocean Ice Studies (JOIS, Fisheries and Oceans Canada at the Institute of Ocean Sciences) program and the Beaufort Gyre Exploration Program (BGEP, Woods Hole Oceanographic Institution; <http://www.whoi.edu/beaufortgyre>). Special thanks to Chief Scientist Sarah Zimmermann for her help and support, including valuable comments on the manuscript, as well as to those who stood in the cold to release drifters at night. Igor E. Kozlov acknowledges the support from RFBF under grant 16–35–60072 mol_a_dk. We are grateful for valuable discussions during the Forum for Arctic Modeling and Observational Synthesis (FAMOS).

References

- Babiano, A., Basdevant, C., Le Roy, P., & Sadourny, R. (1990). Relative dispersion in two-dimensional turbulence. *Journal of Fluid Mechanics*, 214, 535–557. <https://doi.org/10.1017/S0022112090000258>
- Blumen, W. (1978). Uniform potential vorticity flow: Part I. Theory of wave interactions and two-dimensional turbulence. *Journal of the Atmospheric Sciences*, 35, 774–783. [https://doi.org/10.1175/1520-0469\(1978\)035<0774:UPVFP1>2.0.CO;2](https://doi.org/10.1175/1520-0469(1978)035<0774:UPVFP1>2.0.CO;2)
- Boyd, J. (1992). The energy spectrum of fronts: Time evolution of shocks in Burger's equation. *Journal of the Atmospheric Sciences*, 49(2), 128–139. [https://doi.org/10.1175/1520-0469\(1992\)049<0128:TESOFT>2.0.CO;2](https://doi.org/10.1175/1520-0469(1992)049<0128:TESOFT>2.0.CO;2)
- Callies, J., Ferrari, R., Klymak, J. M., & Gula, J. (2015). Seasonality in submesoscale turbulence. *Nature Communications*, 6, 6862. <https://doi.org/10.1038/ncomms7862>
- Capet, X., Campos, E. J., & Paiva, A. M. (2008b). Submesoscale activity over the Argentinian shelf. *Geophysical Research Letters*, 35, L15605. <https://doi.org/10.1029/2008GL034736>
- Capet, X., McWilliams, J. C., Molemaker, M. J., & Shchepetkin, A. F. (2008a). Mesoscale to submesoscale transition in the California Current system. Part I: Flow structure, eddy flux, and observational tests. *Journal of Physical Oceanography*, 38(1), 29–43. <https://doi.org/10.1175/2007JPO3671.1>
- Curcic, M., Chen, S. S., & Ozgokmen, T. M. (2016). Hurricane-induced ocean waves and Stokes drift and their impacts on surface transport and dispersion in the Gulf of Mexico. *Geophysical Research Letters*, 43, 2773–2781. <https://doi.org/10.1002/2015GL067619>
- D'Asaro, E. A., Lee, C., Rainville, L., Harcourt, R., & Thomas, L. (2011). Enhanced turbulence and energy dissipation at ocean fronts. *Science*, 332(6027), 318–322. <https://doi.org/10.1126/science.1201515>
- Haza, A. C., Özgökmen, T. M., Griffa, A., Poje, A. C., & Lelong, M.-P. (2014). How does drifter position uncertainty affect Ocean dispersion estimates? *Journal of Atmospheric and Oceanic Technology*, 31(12), 2809–2828.
- Klein, P., & Lapeyre, G. (2009). The oceanic vertical pump induced by mesoscale and submesoscale turbulence. *Annual Review of Marine Science*, 1(1), 351–375. <https://doi.org/10.1146/annurev.marine.010908.163704>
- Kolmogorov, A. (1941). Dissipation of energy in locally isotropic turbulence. *Proceedings: Mathematical and Physical Sciences*, 434(1890), 15–17.
- Kolmogorov, A. N. (1991). The local structure of turbulence in incompressible viscous fluid for very large Reynolds numbers. *Proceedings: Mathematical and Physical Sciences*, 434(1890), 9–13. <https://doi.org/10.1098/rspa.1991.0075>
- LaCasce, J. (2008). Statistics from Lagrangian observations. *Progress in Oceanography*, 77(1), 1–29. <https://doi.org/10.1016/j.pocean.2008.02.002>
- Lapeyre, G., & Klein, P. (2006). Dynamics of the upper oceanic layers in terms of surface quasigeostrophy theory. *Journal of Physical Oceanography*, 36(2), 165–176.
- Lumpkin, R., Özgökmen, T. M., & Centurioni, L. (2017). Advances in the application of surface drifters. *Annual Review of Marine Science*, 9(1), 59–81. <https://doi.org/10.1146/annurev-marine-010816-060641>
- Luo, H., Bracco, A., Cardona, Y., & McWilliams, J. C. (2016). Submesoscale circulation in the Northern Gulf of Mexico: Surface processes and the impact of the freshwater river input. *Ocean Modelling*, 101, 68–82. <https://doi.org/10.1016/j.ocemod.2016.03.003>
- Mahadevan, A., & Archer, D. (2000). Modeling the impact of fronts and mesoscale circulation on the nutrient supply and biogeochemistry of the upper ocean. *Journal of Geophysical Research*, 105, 1209–1225.
- Mahadevan, A., & Tandon, A. (2006). An analysis of mechanisms for submesoscale vertical motion at ocean fronts. *Ocean Modelling*, 14(3–4), 241–256. <https://doi.org/10.1016/j.ocemod.2006.05.006>
- Manucharyan, G. E., & Thompson, A. F. (2017). Submesoscale sea ice-ocean interactions in marginal ice zones. *Journal of Geophysical Research: Oceans*, 122, 9455–9475. <https://doi.org/10.1002/2017JC012895>
- Martin, A. P., & Richards, K. J. (2001). Mechanisms for vertical nutrient transport within a North Atlantic mesoscale eddy. *Deep-Sea Research, Part II*, 48(4–5), 757–773. [https://doi.org/10.1016/S0967-0645\(00\)00096-5](https://doi.org/10.1016/S0967-0645(00)00096-5)
- McWilliams, J. C. (2008). Fluid dynamics at the margin of rotational control. *Environmental Fluid Mechanics*, 8(5–6), 441–449. <https://doi.org/10.1007/s10652-008-9081-8>
- Mensa, J. A., Garraffo, Z. D., Griffa, A., Özgökmen, T. M., Haza, A. C., & Veneziani, M. (2013). Seasonality of the submesoscale dynamics in the Gulf Stream region. *Ocean Dynamics*, 63(8), 923–941. <https://doi.org/10.1007/s10236-013-0633-1>

- Mensa, J. A., Özgökmen, T. M., Poje, A. C., & Imberger, J. (2015). Material transport in a convective surface mixed layer under weak wind forcing. *Ocean Modelling*, *96*, 226–242. <https://doi.org/10.1016/j.ocemod.2015.10.006>
- Mensa, J. A., & Timmermans, M.-L. (2017). Characterizing the seasonal cycle of upper-ocean flows under multi-year sea ice. *Ocean Modelling*, *113*, 115–130. <https://doi.org/10.1016/j.ocemod.2017.03.009>
- Molemaker, M. J., McWilliams, J. C., & Yavneh, I. (2005). Baroclinic instability and loss of balance. *Journal of Physical Oceanography*, *35*(9), 1505–1517. <https://doi.org/10.1175/JPO2770.1>
- Nicolleau, F. C. G. A., & Nowakowski, A. F. (2011). Presence of a Richardson's regime in kinematic simulations. *Physical Review E*, *83*(5), 1–10. <https://doi.org/10.1103/PhysRevE.83.056317>
- Novelli, G., Guigand, C., Cousin, C., Ryan, E., Laxague, N. J. M., Dai, H., et al. (2017). A biodegradable surface drifter for ocean sampling on a massive scale. *Journal of Atmospheric and Oceanic Technology*, *34*, 2509–2523. <https://doi.org/10.1175/JTECH-D-17-0055.1>
- Okubo, A. (1970). Horizontal dispersion of floatable particles in the vicinity of velocity singularities such as convergences. *Deep Sea Research and Oceanographic Abstracts*, *17*, 445–454. [https://doi.org/10.1016/0011-7471\(70\)90059-8](https://doi.org/10.1016/0011-7471(70)90059-8)
- Omand, M. M., Asaro, E. A. D., Lee, C. M., Perry, M. J., Briggs, N., Cetini, I., et al. (2015). Eddy-driven subduction exports particulate organic carbon from the spring bloom: Supplementary Materials. *Science*, *348*, 1–35. <https://doi.org/10.1126/science.1260062>
- Poje, A. C., Özgökmen, T. M., Bogucki, D. J., & Kirwan, A. D. (2017). Evidence of a forward energy cascade and Kolmogorov self-similarity in submesoscale ocean surface drifter observations. *Physics of Fluids*, *29*(2), 020701. <https://doi.org/10.1063/1.4974331>
- Poje, A. C., Özgökmen, T. M., Lipphardt, B. L., Haus, B. K., Ryan, E. H., Haza, A. C., et al. (2014). Submesoscale dispersion in the vicinity of the Deepwater Horizon spill. *Proceedings of the National Academy of Sciences of the United States of America*, *111*(35), 12693–12698. <https://doi.org/10.1073/pnas.1402452111>
- Proshutinsky, A., Krishfield, R., Timmermans, M.-L., Toole, J., Carmack, E., McLaughlin, F., et al. (2009). Beaufort Gyre freshwater reservoir: State and variability from observations. *Journal of Geophysical Research*, *114*, C00A10. <https://doi.org/10.1029/2008JC005104>
- Richardson, L. (1926). Atmospheric diffusion shown on a distance-neighbour graph. *Proceedings of the Royal Society of London. Series A*, *110*(756), 709–737.
- Rudnick, D. (1996). Intensive surveys of the Azores Front 2. Inferring the geostrophic and vertical velocity fields. *Journal of Geophysical Research*, *101*, 16291–16303.
- Sasaki, H., Klein, P., Qiu, B., & Sasai, Y. (2014). Impact of oceanic-scale interactions on the seasonal modulation of ocean dynamics by the atmosphere. *Nature Communications*, *5*, 5636. <https://doi.org/10.1038/ncomms6636>
- Shcherbina, A. Y., D'asaro, E. A., Lee, C. M., Klymak, J. M., Molemaker, M. J., & McWilliams, J. C. (2013). Statistics of vertical vorticity, divergence, and strain in a developed submesoscale turbulence field. *Geophysical Research Letters*, *40*, 4706–4711. <https://doi.org/10.1002/grl.50919>
- Thomson, D. J., & Devenish, B. J. (2005). Particle pair separation in kinematic simulations. *Journal of Fluid Mechanics*, *526*(2005), 277–302. <https://doi.org/10.1017/S0022112004002915>
- Timmermans, M.-L., Cole, S., & Toole, J. (2012). Horizontal density structure and restratification of the Arctic Ocean surface layer. *Journal of Physical Oceanography*, *42*(4), 659–668. <https://doi.org/10.1175/JPO-D-11-0125.1>
- Timmermans, M.-L., & Winsor, P. (2013). Scales of horizontal density structure in the Chukchi Sea surface layer. *Continental Shelf Research*, *52*, 39–45. <https://doi.org/10.1016/j.csr.2012.10.015>
- Veneziani, M., Griffa, A., Reynolds, A., & Mariano, A. (2004). Oceanic turbulence and stochastic models from subsurface Lagrangian data for the Northwest Atlantic Ocean. *Journal of Physical Oceanography*, *34*(8), 1884–1906.
- Zhao, M., Timmermans, M.-L., Cole, S., Krishfield, R., Proshutinsky, A., & Toole, J. (2014). Characterizing the eddy field in the Arctic Ocean halocline. *Journal of Geophysical Research: Oceans*, *119*, 8800–8817. <https://doi.org/10.1002/2014JC010488>